Chapter 5

Design of a $Q = 5$ tokamak

5.1 Introduction

In the framework of the prospective studies for the next step of the fusion program, the Euratom-CEA Association was asked to examine the design basis of an European tokamak machine as an alternative to ITER, should ITER be abandoned or delayed for a long time. The main aim of this machine, called M2, is the study of plasma physics in a reactor perspective within the limited European budget (less than 2 billion Euros). This leads to the choice of an amplification factor $Q \sim 5$, which is considered to be the minimum value for the study, under good conditions, of the internal heating by the alpha particles[1]. Such a machine would be part of a multi-step strategy, which would lead to significantly increasing the overall cost and the time frame to arrive at a demonstration reactor compared to the ITER-type strategy.

In this Chapter the parameters of the M2 machine are optimized in order to determine the smallest machine, for a given aspect ratio, generating a $Q = 5$ plasma in inductive mode of operation with a burn duration of about 500 seconds, meeting the physical and technological requirements. These physical and technological requirements are close to those of ITER, since they are widely accepted by the scientific community.

The M2 machine would also provide:

- The study of the control and maintenance of stationary discharges.
- The validation of non-inductive current generation methods, which play a fundamental part in the control of stationary discharges.
- The study of the edge plasma namely the operation of the divertor and the pumping of helium.

[1] The alpha power heating is roughly equal to the external power heating for $Q = 5$.

- The exploration of advanced tokamak concepts.
- The validation of both the fusion energy at a significant power lever (several hundreds of MW) and the safety conditions.

Compared with the ITER objectives, this M2 next step would not explore the massive plasma heating by the alpha particles ($Q = 5$ for M2 is compared to $Q = 10$ for ITER-FEAT, in inductive operation). Moreover, no objectives in terms of qualification of materials under large fluence of neutrons are specified for M2. This machine would then mostly use tested and reliable technologies, allowing a reduction of construction costs. This experimental M2 machine is predicted to operate for 15 years, with 1000 shots of 500 seconds per year, and with 1/3 of the shots in D-T.

5.2 Tools for tokamak design

We use the HELIOS code, which implements the plasma model described in Chapter 1, for the modelling of plasma physics and the ESCORT code (Electromagnetic Superconducting System for the Computation Of Research Tokamaks) for the magnet system design [Duc99c].

5.2.1 Physics model

The optimisation study of the M2 device has been performed using the same set of physics assumptions as those of ITER-FDR [FDR97].

First, the thermal equilibrium equation (Eq. (2.1)) is solved by describing the conductive-convective transport losses P_{con} with the empirical global energy confinement time τ_E. The empirical expression used for the calculation of τ_E is the ITERH-97P(ELMy) scaling ($\tau_E = \tau_{E,\text{ITERH-97P(ELMy)}}$), derived from the analysis of the 1997 international dataset for the ELMy H-mode regime:

$$\tau_{E\text{ITERH-97P(ELMy)}} = 2.9 \times 10^{-11.04} \frac{M_{\text{eff}}^{0.2}\ \kappa_X^{0.92}\ I_p^{0.9}\ (\overline{n}_e)^{0.4}\ B_{t_0}^{0.2}\ R^{1.84}\ a^{0.19}}{P_{\text{net}}^{0.66}}. \quad (5.1)$$

Next, we consider the ITER-FDR expression for the H-L transition power threshold including the atomic mass M_{eff} effect observed in JET discharges:

$$P_{\text{H-L (FDR)}} = 9 \times 10^{-10}\,(\overline{n}_e)^{0.75}\,B_{t_0} R^2 M_{\text{eff}}^{-1}.$$

In this approach, we neglect the radiated power at the plasma edge inside the separatrix $P_{\text{rad-mantle}}$, leading to $P_{\text{con}} = P_{\text{sep}}$. This assumption corresponds to the case where the temperature pedestal in H-mode is high enough for light impurities not to radiate any longer, and where radiative impurities are not injected.

For the operating temperatures of the M2 plasmas ($T_e < 10$ keV) we will see in Section 5.6 that synchrotron radiation losses are low with respect to the total losses. In this optimisation study, we have neglected this term in the thermal equilibrium of the plasma.

Finally, the following assumptions are made concerning the plasma shaping, density and temperature profiles, and impurities:

- The elongation at the 95% magnetic flux surface is supposed to depend on the aspect ratio A as follows:

  $$\kappa_{95} = 2.22 - 0.17A,$$

  in order to include a simple criterion for the plasma vertical stability deduced from ITER aspect ratio studies [RTO98]. The elongation at the X-point is taken to be

  $$\kappa_X = 1.11 \times \kappa_{95}$$

  with a constant triangularity

  $$\delta_{95} = \delta_X = 0.35.$$

- The Beryllium and Argon plasma core content are taken to be the nominal ITER-FDR values ($f_{\text{Be}} = 2\%$, $f_{\text{Ar}} = 0.16\%$). For the study in inductive mode of operation, we consider a constant helium fraction $f_{\text{He}} = 2\%$, which corresponds to a ratio of the apparent helium confinement time to the energy confinement time about 6 ($\tau^*_{\text{He}}/\tau_E \simeq 6$), giving $Z_{\text{eff}} \simeq 1.77$. For the non-inductive mode of operation (current drive operation) we impose $\tau^*_{\text{He}}/\tau_E = 6$.

- The density and temperature profiles in H-mode regime are in agreement with ITER-FDR when we take $\alpha_n = 0.01$ and $\alpha_T = 1.3$ for the generalized parabolic profiles described by Eq. (3.25).

  All plasma ions have a temperature 10% lower than the electron temperature T_e.

5.2.2 Technical basis description of the magnetic systems

The main technical lines of the superconducting machine are close to those of ITER since they are widely accepted by the scientific community. Therefore, the vault concept is chosen for the toroidal field (TF) system. The central solenoid (CS) is independent from the TF system. The CS and the TF magnets are made of Nb^3Sn at 4.75 K (with a margin of 1 K), while the poloidal field (PF) system is made of NbTi (with a margin of 2 K). All conductors of the magnetic systems are circular cables inserted in a square steel jacket.

The basic method used for the design of the tokamak magnetic systems is the radial build. This method lies in describing sequentially, on the equatorial plane, all the elements forming the tokamak, from the plasma centre to the vertical tokamak axis (points separated by a distance R). Fig. 5.1 shows the main tokamak dimensions in the equatorial plane.

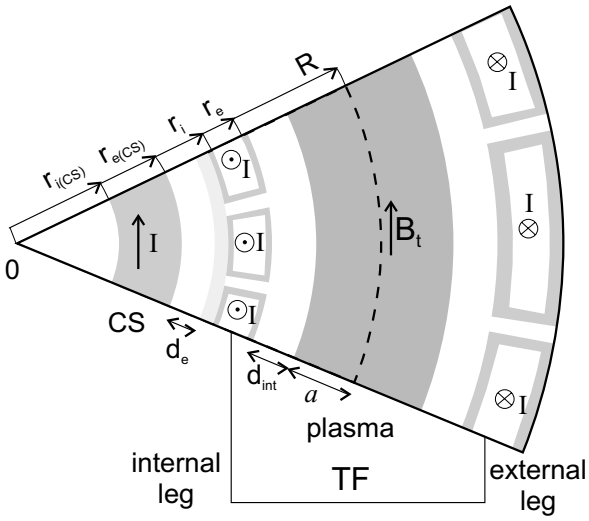

Figure 5.1: Schematic diagram of the main elements in the equatorial plane of a tokamak.

Describing sequentially the different elements from the plasma centre to the tokamak axis 0, we have first the plasma scrape-off layer, the internal first wall, the internal cryostat, and the internal vacuum vessel, respectively, followed by the internal leg of the toroidal field coils. Note that the internal first wall should be designed to limit the thermal load and the neutron power density on the TF magnets [Ane98]. In this study, we take a constant ITER-like value for the first wall depth of 0.6 m (which is conservative since M2 has a fusion power and an energy contents lower than those of ITER-FEAT). The distance between the plasma and the internal leg of the TF coil is denoted as d_{int}, which is taken to be $d_{\text{int}} = 0.9$ m in the present study.

The TF winding plus the vault structure give the total thickness of the TF internal leg, as shown in Fig. 5.2. Then, there is the external cryostat and vacuum vessel with a thickness $d_e = 0.1$ m, followed by the central solenoid CS.

Superconducting conductor: The design criteria selected are those of ITER. All the conductors use a model conductor coil with a circular cable-in-conduit with a central cooling channel, which allows the 4.75K supercritical helium to circulate

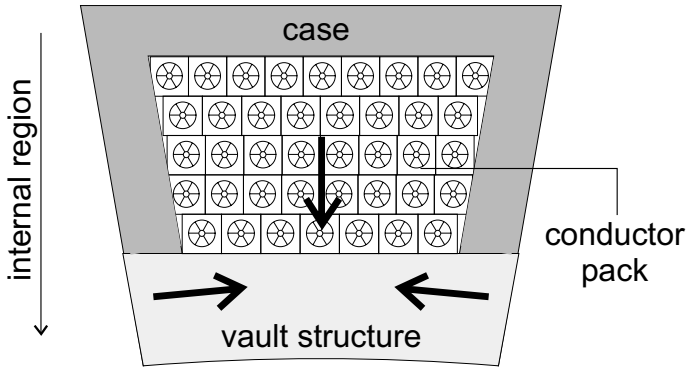

Figure 5.2: Schematic drawing of the internal leg TF coil and the centering force transmission in the equatorial plane.

with a low pressure drop. As seen in Fig. 5.3, the cable is made up of 6 petals around the central hole and inserted in a square steel jacket.

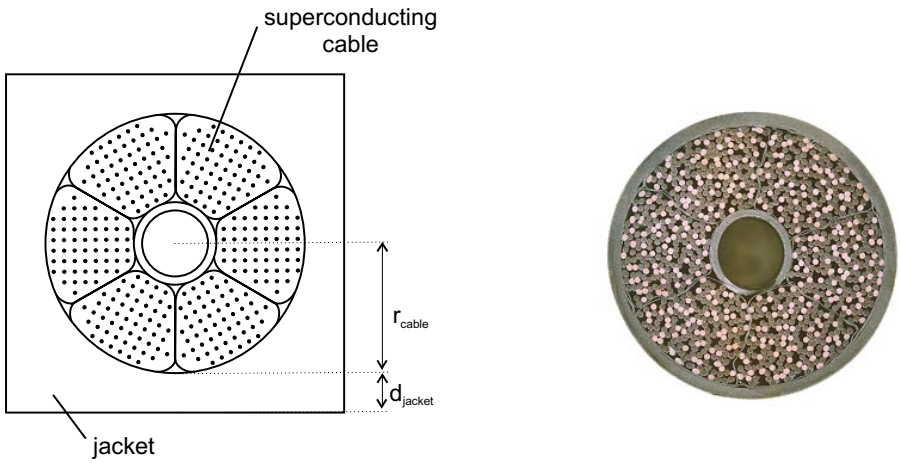

Figure 5.3: On the left, schematic conductor model of the M2 coils. On the right, the cable of the Toroidal Field Model Coil for ITER, manufactured by the AGAN Consortium (Ansaldo, Noell, Alstom) [Duc99a].

Typical achievable cable current densities according to the superconducting material and the operating temperature are presented in Fig. 5.4.

Toroidal field system: The magnetic field at the plasma axis B_{t0} is related to the maximum magnetic field on the TF conductor $B_{t\,\max}$ (at the r_e radius in Fig. 5.1) by

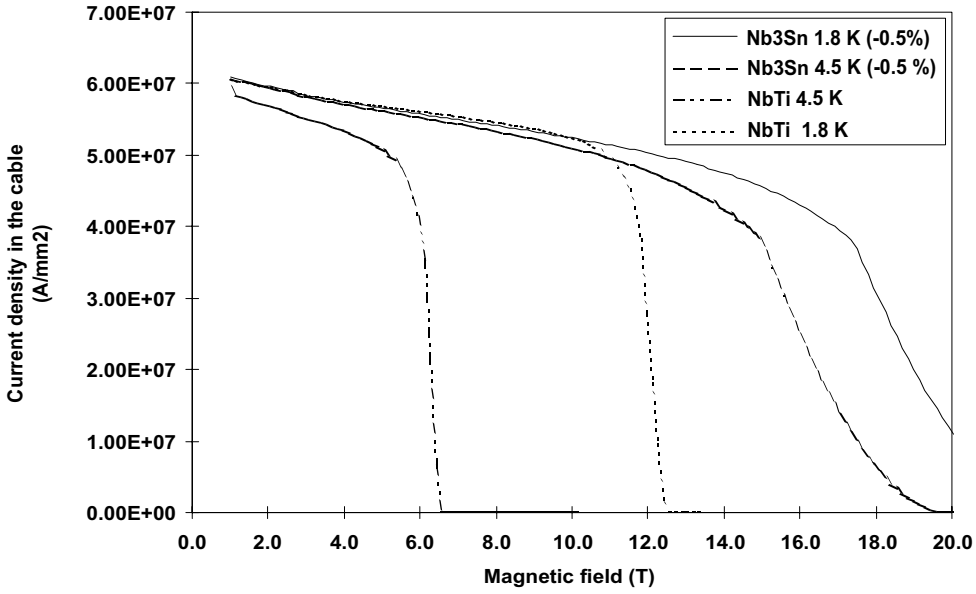

Figure 5.4: Current density in a cable-in-conduit as a function of the superconducting material (Nb^3Sn or NbTi) and of the operating temperature (source: Ref. [Duc99a][Duc99b]).

means of Ampere's law, as follows:

$$\frac{B_{t_0}}{B_{t\,\max}} = \frac{A - 1 - \Delta_{\text{int}}/a}{A}$$

where Δ_{int} is d_{int} increased 0.1 m by the thickness of the case of the toroidal coils. Thus, we have $\Delta_{\text{int}} = 1$ m.

The most restrictive condition in the toroidal field TF system is the mechanical constraint at the internal row of conductors, i.e. at the r_i radius in Fig. 5.1. Here, it is possible to distinguish two main mechanical constraints [Duc99b]: first of all, the centring pressure

$$\sigma_{\text{centring}} = \frac{2r_e^2 B_{t_1\,\max}^2 \left(r_e^3 + 2r_i^3 - 3r_i^2 r_e\right)}{3\mu_0 r_i \left(r_e^2 - r_i^2\right)^2} f, \tag{5.2}$$

where r_e is the external radius of the internal leg TF winding[2], r_i is the internal radius of the internal leg TF winding, $B_{t_1\,\max}$ is the maximum magnetic field increased by the ripple effect (around 10%), and f is the amplifying factor (transmission of the centring force through the jacket, which acts as a structural material):

$$f = \frac{\left(r_{\text{cable}} + d_{\text{insu}} + d_{\text{jacket}}\right)}{d_{\text{jacket}}}, \tag{5.3}$$

[2]Distances measured from the vertical tokamak axis.

where r_{cable} is the cable radius, d_{insu} the insulating thickness ($d_{\text{insu}} = 2 \times 10^{-3}$ m), and d_{jacket} is the jacket thickness (see Fig. 5.3). Secondly, the hoop constraint:

$$\sigma_{\text{hoop}} = \frac{B_{t_1\,\max}^2}{2\mu_0} \frac{r_e^2}{r_1 \delta} \frac{K}{F},$$

where r_1 is the average radius of the internal TF leg, r_2 is the average radius of the external TF leg, δ is the winding thickness, F is the structural ratio in the winding pack, and $K = 1/2 \ln(r_2/r_1)$. A typical value of σ_{hoop} is about 100 MPa.

The Tresca constraint is defined as $\sigma_{\text{Tresca}} = \sigma_{\text{centring}} + \sigma_{\text{hoop}}$, and according to ITER design criteria we impose

$$\sigma_{\text{Tresca}} \leq \frac{2}{3} \sigma_{\text{yield}},$$

which leads to $\sigma_{\text{Tresca}} \leq$ 600 MPa for the jacket supporting the centring force at the conductor internal row.

An important consequence of the dependence of the cable current density on the magnetic field, and of the mechanical constraints is the non-linear increasing of the TF thickness when the required $B_{t\,\max}$ increases. Indeed, more superconducting cable is needed to generate the higher $B_{t\,\max}$, but, as seen in Fig. 5.4, the cable current density decreases when $B_{t\,\max}$ increases. Thus, a thicker winding pack is further needed to generate $B_{t\,\max}$. Adding to this effect and according to Eq. (5.2), the centring pressure also increases due to the lower value of r_i and, as a result, more structural steel is required (bigger jackets) increasing even more the TF thickness. These multiplication effects make the toroidal field system design very sensitive to the value of the magnetic field, resulting in no design solution for high values of $B_{t\,\max}$.

The external part of the TF magnets is designed with a closed D shape which ensures a ripple of 1% at the edge of the plasma.

Vault system: The vault structure is a support cylinder located immediately after the TF winding pack, where the mechanical constraints are highest. The centring force of the TF winding is transmitted through conductor jackets to the inner nose of the coils, making up the vault, and the centring force is transformed into an implosion force (as shown in Fig. 5.2). The maximum design Tresca constraint is $\sigma_{\text{Tresca,max}}^{(\text{v})} = 700$ MPa for the vault.

The internal radius of the vault r_i' can be determined from the internal radius of the TF winding pack r_i through the following formula:

$$r_i' = r_i^2 \left(1 - \frac{2\sigma_{\text{centring}}}{f\ \sigma_{\text{Tresca}}^{(\text{v})}} \right)$$

with σ_{centring} and f given in Eqs (5.2) and (5.3), respectively.

Central solenoid and poloidal field system: The central solenoid (CS) generates the available magnetic flux whose variation will induce the plasma current in the inductive mode of operation. This CS system fills the central space available between the external vacuum vessel and the tokamak axis. It is mechanically independent from the TF system due to the presence of the vault structure.

The CS is designed in order to maximize the available magnetic flux, taking into account the superconducting current density versus the magnetic field (lower than 13.5 T), the space available, and the quantity of steel structural material in the CS conductors required for compensating the explosion force (as seen in the TF system), which is subjected to mechanical cycling.

Finally, the external poloidal field (PF) coils are designed [Duc99c].

The plateau flux consumption Ψ_{plateau} is the flux left over from the total reserve of poloidal flux (contributions of the central solenoid flux Ψ_{CS} and vertical flux Ψ_{vert}) once the plasma has been initiated and the ramp-up flux has been consumed, i.e.

$$\Psi_{\text{plateau}} = \Psi_{\text{CS}} + \Psi_{\text{vert}} - \Psi_{\text{ind}} - \Psi_{\text{res}} - \Psi_{\text{break}},$$

where Ψ_{break} is the plasma initiation flux consumption ($\Psi_{\text{break}} \simeq 20$ Wb), and Ψ_{ind} and Ψ_{res} are the inductive and resistive fluxes consumed during the plasma ramp-up, respectively.

Finally, the plateau time t_{plateau} is

$$t_{\text{plateau}} = \frac{\Psi_{\text{plateau}}}{U_\ell},$$

where U_ℓ is the loop voltage ($U_\ell = E\, 2\pi R$). Using Eq. (2.5) for the toroidal electric field E, we obtain

$$U_\ell = 2\pi\eta_0 R\, Z_{\text{eff}} \frac{(I_p - I_{\text{BS}} - I_{\text{CD}})}{\int_S \dfrac{T_e(\rho)^{3/2}}{\ln\Lambda(\rho)\,\gamma_{\text{NC}}\,(\rho)} dS},$$

where $\ln\Lambda$ is the Coulomb logarithm, γ_{NC} is the neo-classical enhancement factor, I_{BS} is the bootstrap current, and I_{CD} is the externally driven current.

5.3 Optimisation algorithm

In the following paragraphs, we describe the algorithm that we have suggested in order to determine the smallest machine for a given aspect ratio $A = R/a$ generating a plasma in H-mode with ELMs and satisfying the following objectives:

- amplification factor $Q = 5$ ($\sim 50\%$ alpha heating, $\sim 50\%$ additional heating),

- length of plateau of 500 seconds ($t_{\text{plateau}} = 500$ s),
- current generated inductively, by imposing the minimum safety factor at the 95% magnetic flux surface authorised by MHD stability, i.e. $q_{\Psi 95} = 3$. This condition allows the maximum plasma current I_p as seen in Eq. (2.29);

with the following physical boundaries, close to those taken for the design basis of ITER-FEAT [ODR99]:

- plasma density equal to 90% of the Greenwald limit ($n_e = 0.9\, n_{\text{Gr}}$),
- conductive power crossing the last closed magnetic surface P_{sep} exceeding by a least 20% the $P_{\text{H-L}}$ power corresponding to the H-L transition ($P_{\text{sep}} \geq 1.2\, P_{\text{H-L}}$),
- beta normalized parameter lower or equal to 2.5 ($\beta_{\text{N}} \leq 2.5$).

We also assume that the current ramp-up is made purely inductively. The technological requirements are as follows:

- $\Delta_{\text{int}} = 1$ m (in the equatorial plane, addition of the thickness of the following elements: plasma scrape-off layer, internal first wall, internal cryostat, internal vacuum vessel, and case of the toroidal coils),
- 18 TF coils made of Nb^3Sn at 4.75 K (with a margin of 1 K),
- ripple at the edge of outside the plasma $< 1\%$,
- maximum mechanical Tresca constraint for the steel (square conductor jackets: 600 MPa, vault: 700 MPa).

For a given aspect ratio (e.g. $A = 3.5$) we take a tentative plasma size (e.g. $R = 4.6$ m). For a too weak magnetic field B_{t_0} on the plasma axis (e.g. $B_{t_0} = 5$ T), we note that the curve $Q = 5$ in the plane $(\langle n_e \rangle, \langle T_e \rangle)$ plane is located entirely above the line $n_e/n_{\text{Gr}} = 0.9$. We then increase the magnetic field and the corresponding plasma current (with $q_{\Psi 95} = 3$) until the curve $Q = 5$ becomes tangent to the line $n_e/n_{\text{Gr}} = 0.9$. If the corresponding operating point meets the requirements $P_{\text{sep}}/P_{\text{H-L}} \geq 1.2$ and $\beta_{\text{N}} \leq 2.5$, we keep the magnetic field; if not, it is increased again until these two conditions ($P_{\text{sep}}/P_{\text{H-L}} \geq 1.2$ and $\beta_{\text{N}} \leq 2.5$) are simultaneously met at the operating point.

For the plasma magnetic field obtained, we calculate the field $B_{t,\max}$ in the superconducting coil corresponding to the plasma considered, by taking into account the ripple effect. Then we calculate the thickness of the toroidal coil, for the maximum current density authorised by $B_{t,\max}$, which allows the generation of $B_{t,\max}$

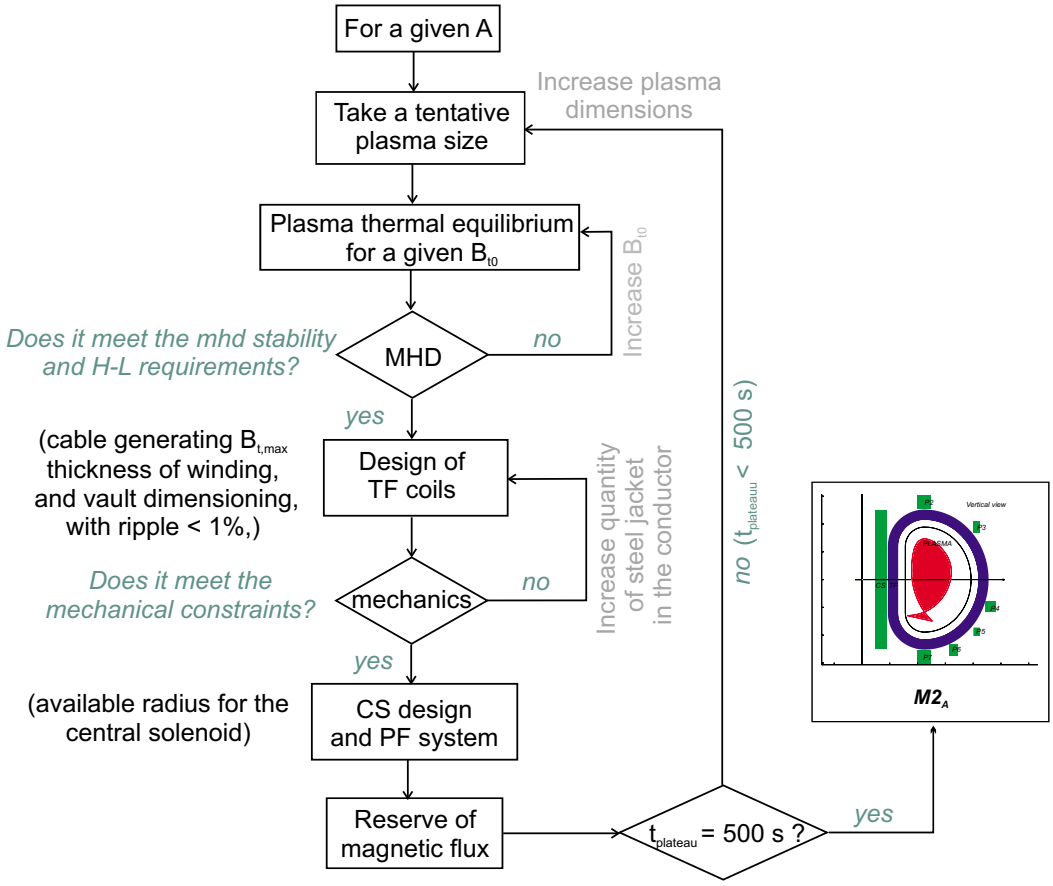

Figure 5.5: Optimisation process diagram for the M2 device.

while meeting the mechanical constraints. The dimensions of the external leg are then calculated to ensure the constraint of maximum ripple outside the plasma.

Having thus obtained the available radius for the central solenoid, we can then design the poloidal coils and calculate the maximum reserve for the poloidal flux. After subtracting the flux necessary for the current break down and ramp-up, we can calculate the duration of the plateau corresponding to the operating point determined in the preceding stage.

If this burning time is lower than 500 seconds, we choose a larger dimension and repeat the algorithm explained above until we obtain a plateau of 500 seconds.

The machine thus determined is therefore the smallest machine meeting the imposed physical and technological requirements.

In Fig. 5.6, the values of B_{t_0} and $B_{t_1\,\max}$ are represented as well as the duration of the plateau versus plasma size, for the fixed aspect ratio $A = 3.5$. When $R < 4.51$ m (orange-coloured zone) the ESCORT code cannot calculate a toroidal magnet

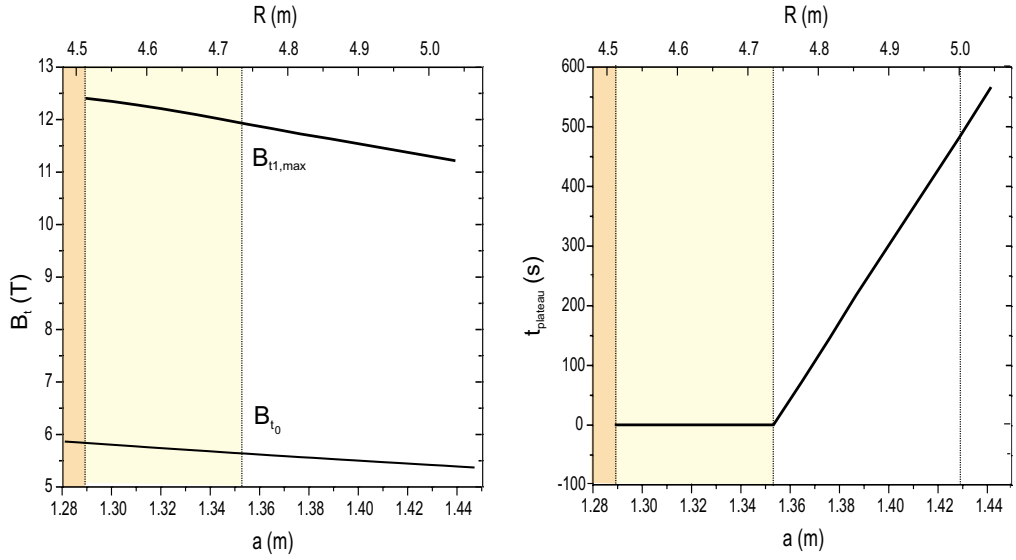

Figure 5.6: Magnetic field on the plasma axisB_{t_0} and maximum magnetic field in the superconducting coil $B_{t_1\,\mathrm{max}}$ increased by the ripple effect (on the left side), and plateau duration t_{plateau} corresponding to the increasing dimension machines of the optimisation algorithm with $A = 3.5$.

meeting the mechanical stresses. For $4.51 < R < 4.72$ m (yellow zone), this magnet does exist, but the poloidal flux available provides only part of the current break down and ramp-up. For $R > 4.72$ m (white zone), the plateau exists and becomes equal to 500 seconds for $R = 5.00$ m.

5.4 Design basis and performance

The optimisation algorithm presented above has been applied for three different aspect ratios: 3, 3.5 and 4. Results are presented in the following Sections.

5.4.1 Aspect ratio $A = 3$

The parameters resulting from the optimisation algorithm for an aspect ratio of A = 3 are:

$$R = 5.24\ \mathrm{m}, \quad a = 1.75\ \mathrm{m}, \quad \kappa_{95} = 1.71, \quad \delta_{95} = 0.35,$$

with the toroidal magnetic field on the plasma axis $B_{t_0} = 4.31$ T.

Fig. 5.7 shows the poloidal section of the plasma and magnetic system of this machine.

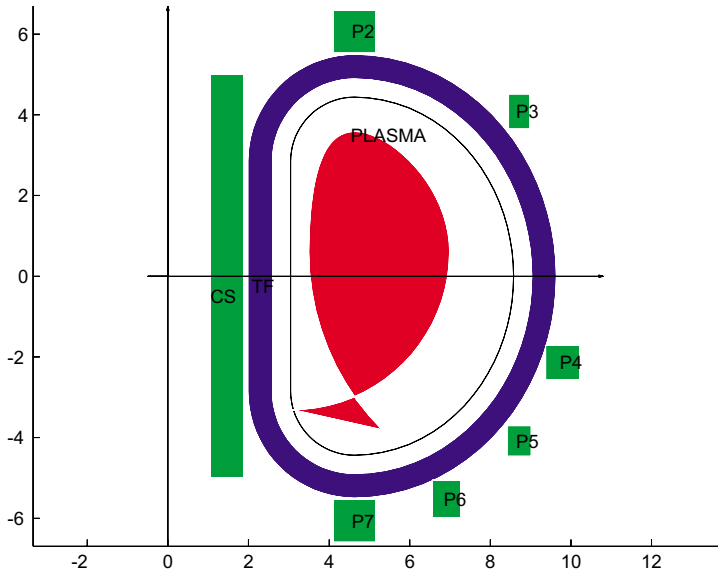

Figure 5.7: Vertical view of the $A = 3$ toroidal and poloidal magnetic systems, and plasma corresponding to $t_{\text{plateau}} = 500$ s.

Inductive mode of operation: Fig. 5.8 shows the performance of the optimized device with an aspect ratio of $A = 3$ in inductive mode of operation, i.e. $q_{\Psi 95} = 3$ giving $I_p \simeq 11.3$ MA. The white area in these plots represents the operating space, which is limited by the transition between the H-mode and L-mode (blue curve) and by the plasma stability constraints, i.e. the Greenwald density limit (green curve) and beta pressure limit (red curve).

The operating point resulting from the optimisation is also shown in the plane ($\langle T \rangle$,$\langle n_e \rangle$) of Fig. 5.8. It corresponds to a 500 seconds burning plasma meeting both $Q = 5$ at $n_e/n_{\text{Gr}} = 0.9$ and the constraints $P_{\text{sep}}/P_{\text{H-L}} \geq 1.2$, $\beta_{\text{N}} \leq 2.5$, with a fusion power of $P_{\text{fus}} \simeq 169$ MW and a peak heat flux on the divertor target plates of $\Phi_{\text{div-peak}} \simeq 6.3$ MW/m^2.

For this aspect ratio, we see that the $Q = 5$ point on the $n_e/n_{\text{Gr}} = 0.9$ curve corresponds to the minimum of the countour $Q = 5$ in the plane ($\langle T_e \rangle$, $\langle n_e \rangle$).

Non-inductive mode of operation: The performance of such a machine is analysed in the non-inductive mode of operation assuming a current drive efficiency proportional to the volume average temperature, as

$$\gamma_{\text{CD}} = \gamma_{0\text{CD}} \langle T \rangle \qquad \text{with} \qquad \gamma_{0\text{CD}} = 0.2 \times 10^{19} \ \text{A m}^{-2}/\left(\text{W keV}\right).$$

For this evaluation, we consider an advanced regime with an enhanced confine-

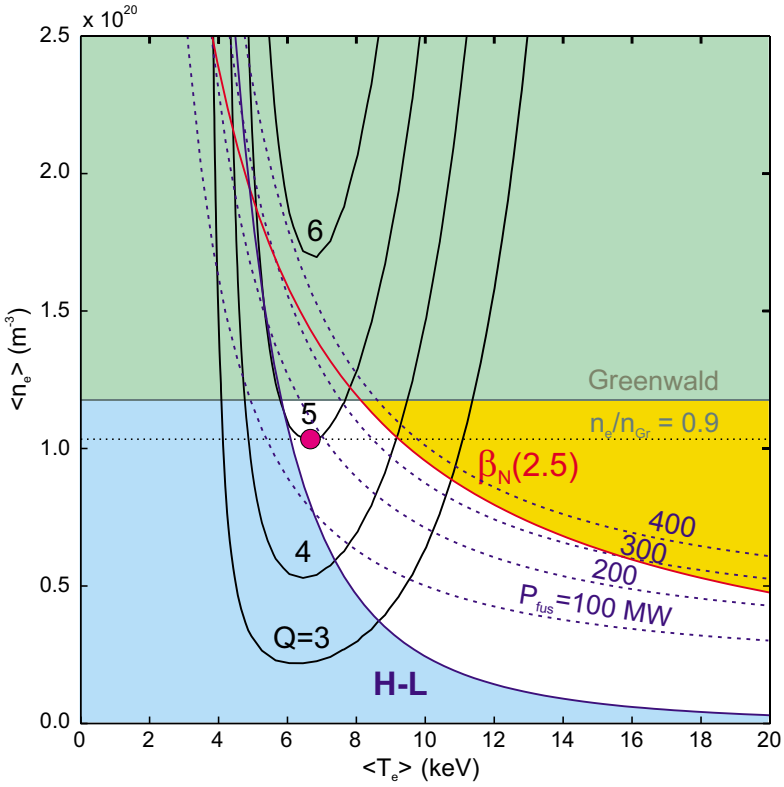

Figure 5.8: Inductive performances of the machine $A = 3$ with $q_{\Psi 95} = 3$ ($I_p \simeq 11.3$ MA).

ment with respect to the ELMy H-mode (Eq. (5.1),

$$H_{\rm H} = 1.4,$$

with a peaking density profile ($\alpha_n = 1.0$). The helium fraction is calculated self-consistently by imposing the ratio of the apparent helium confinement time to the energy confinement time $\tau^*_{\rm He}/\tau_E = 6$.

The current drive diagram is shown in Fig. 5.9. Although at present there is no scaling law for the power threshold required for maintaining the advanced regime, we have plotted the H-L transition curve in the plane $(P_{\rm add}, \langle n_e \rangle)$, only as an additional information. With the above assumptions, the maximum amplification factor is $Q \simeq 4.9$, obtained with a reasonable value of additional heating power ($P_{\rm add} \simeq 43$ MW) and a peak heat flux on the divertor target plates ($\Phi_{\rm div\text{-}peak} \simeq 9.2$ MW/m^2) close to the ITER-FEAT design value (10 MW/m^2).

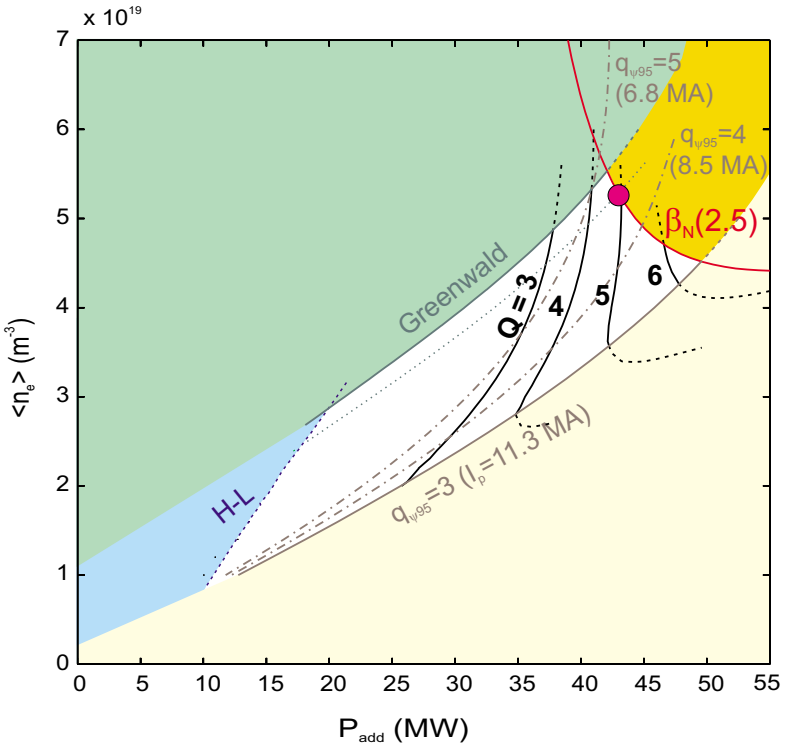

Figure 5.9: Current drive diagram of the $A = 3$ device considering an advanced tokamak regime ($H_{\mathrm{H}} = 1.4$ and $\alpha_n = 1.0$).

5.4.2 Aspect ratio $A = 3.5$

The resulting optimized parameters for an aspect ratio $A = 3.5$ machine are as follows:

$$R = 5.00 \text{ m}, \quad a = 1.43 \text{ m}, \quad \kappa_{95} = 1.63, \quad \delta_{95} = 0.35,$$

with the toroidal magnetic field on the plasma axis $B_{t_0} = 5.43$ T.

Fig. 5.10 shows the poloidal section of the plasma and magnetic system of this machine with $A = 3.5$, where we notice that the TF coil is thicker than that of the $A = 3$ machine. Indeed, when A increases, the internal space available for the toroidal field and central solenoid grows. Then, by maintaining the magnetic flux required for generating a plateau time of 500 seconds, the TF can be made thicker and the magnetic field (both on the TF conductor and on the plasma) higher. Finally, for given physical constraints and $Q = 5$ objective, the plasma dimensions are smaller when the magnetic field increases, fulfilling the purpose of the optimisation.

Inductive mode of operation: Fig. 5.11 shows the performance of the optimized device with an aspect ratio of $A = 3.5$ in inductive mode of operation, i.e. $q_{\Psi 95} = 3$

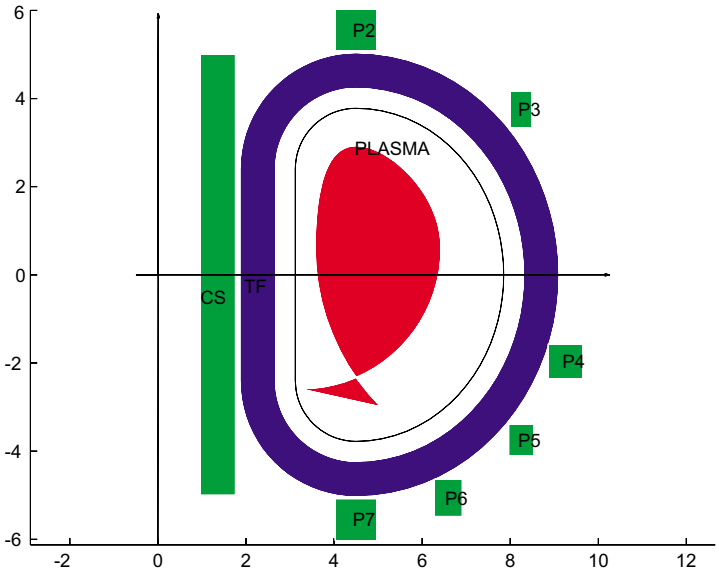

Figure 5.10: Vertical view of the $A = 3.5$ toroidal and poloidal magnetic systems, and plasma corresponding to $t_{\text{plateau}} = 500$ s.

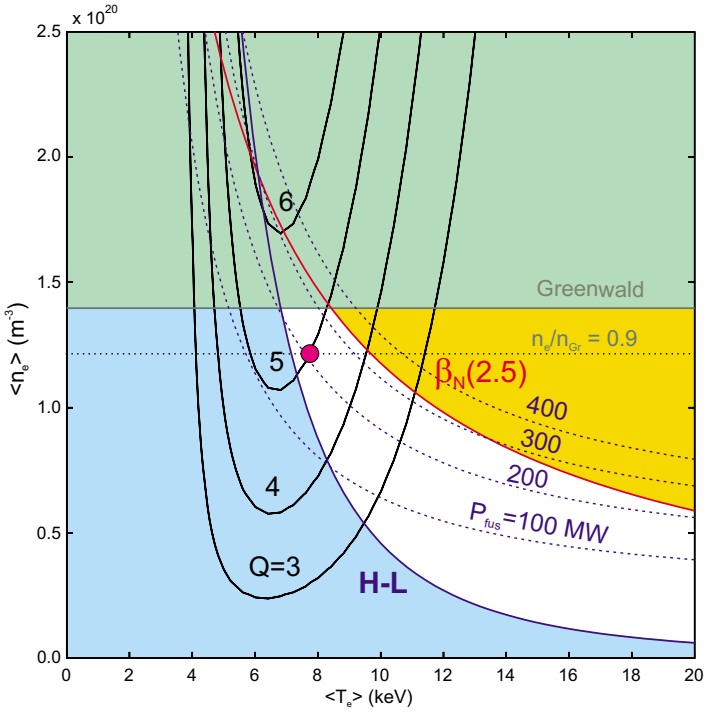

Figure 5.11: Inductive performances of the machine $A = 3.5$ with $q_{\Psi 95} = 3$ ($I_p \simeq 9.0$ MA).

giving $I_p \simeq 9.0$ MA. Now, we see that the $Q = 5$ point on the $n_e/n_{\text{Gr}} = 0.9$ curve is located on the $P_{\text{sep}}/P_{\text{H-L}} = 1.2$ curve, and it corresponds to a fusion power of $P_{\text{fus}} \simeq 206$ MW and to a peak heat flux on the divertor target plates of $\Phi_{\text{div-peak}} \simeq 8.6$ MW/m^2 (meeting the ITER-FEAT constraint).

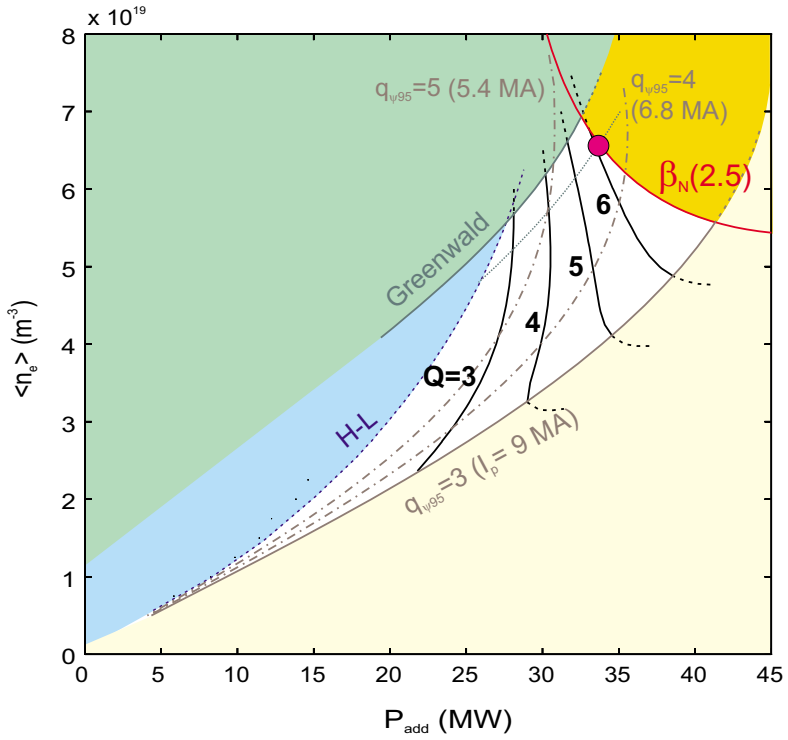

Figure 5.12: Current drive diagram of the $A = 3.5$ device considering an advanced tokamak regime ($H_{\text{H}} = 1.4$ and $\alpha_n = 1.0$).

Non-inductive mode of operation: The current drive diagram for this $A = 3.5$ device considering an advanced regime ($H_{\text{H}} = 1.4$ and $\alpha_n = 1.0$) is shown in Fig. 5.12. With the above assumptions, the maximum amplification factor is increased to $Q \simeq 6.1$ with respect to the $A = 3$ device and, for this point, $\Phi_{\text{div-peak}}$ is softly reduced to about 9 MW/m^2.

5.4.3 Aspect ratio $A = 4$

The resulting optimized parameters for the $A = 4$ machine are as follows:

$$R = 5.02 \text{ m}, \quad a = 1.26 \text{ m}, \quad \kappa_{95} = 1.54, \quad \delta_{95} = 0.35,$$

with the toroidal magnetic field on the plasma axis $B_{t_0} = 6.56$ T.

Fig. 5.13 shows the poloidal section of the plasma and magnetic system of this machine. We see that the TF coil is thicker than those of the lower aspect ratios ($A = 3$ and 3.5) due to the higher magnetic field.

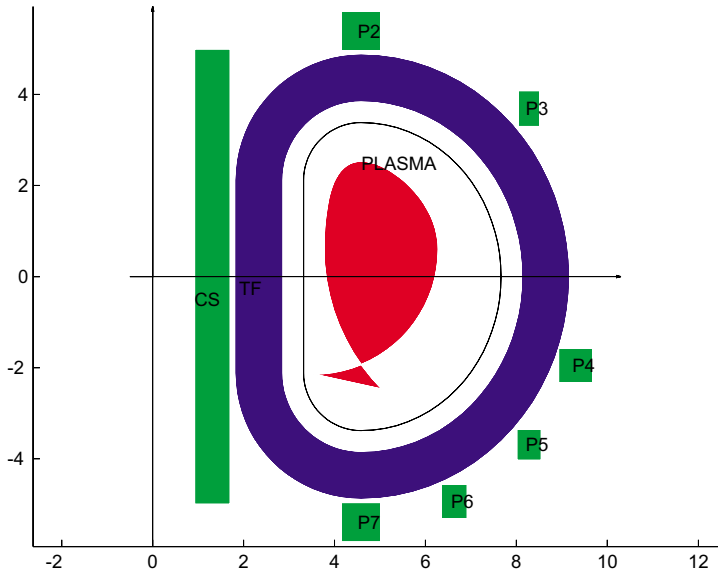

Figure 5.13: Vertical view of the $A = 4$ toroidal and poloidal magnetic systems, and plasma corresponding to $t_{\text{plateau}} = 500$ s.

Inductive mode of operation: Fig. 5.14 shows the performance of the optimized device with an aspect ratio of $A = 4$, in inductive mode of operation, i.e. $q_{\Psi 95} = 3$ giving $I_p \simeq 7.5$ MA.

As for the $A = 3.5$ device, the $Q = 5$ nominal point is located on the $P_{\text{sep}}/P_{\text{H-L}} = 1.2$ curve. The corresponding fusion power is $P_{\text{fus}} \simeq 260$ MW, and the peak heat flux on the divertor target plates ($\Phi_{\text{div-peak}} \simeq 11$ MW/m^2) becomes higher than the ITER-FEAT constraint. We also notice that the operating space in the plane ($\langle T_e \rangle$, $\langle n_e \rangle$) is narrower than those corresponding to $A = 3$ or 3.5.

Non-inductive mode of operation: The current drive diagram for this $A = 4$ device considering an advanced regime ($H_{\text{H}} = 1.4$ and $\alpha_n = 1.0$) is shown in Fig. 5.15. With the above assumptions, the maximum amplification factor is significantly increased to $Q \simeq 8.0$ and, for this point, $\Phi_{\text{div-peak}}$ is softly reduced to about 7.8 MW/m^2.

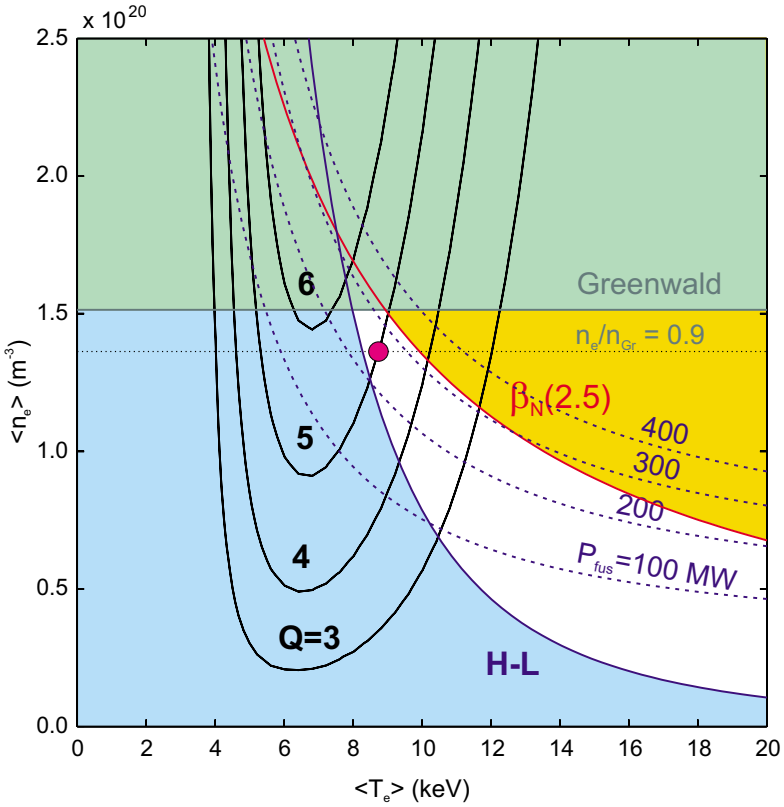

Figure 5.14: Inductive performances of the machine $A = 4$ with $q_{\Psi 95} = 3$ ($I_p \simeq 7.5$ MA).

5.5 Comparison of the optimized machines at aspect ratios 3, 3.5 and 4

The optimisation process in the inductive mode of operation, considering the physical and technological constraints of Section 5.2, leads to the tokamak parameters presented in Table 5.1 for aspect ratios 3, 3.5 and 4.

Table 5.2 presents the characteristics of the operating point in current drive operation (non-inductive) with an advanced scenario, for each optimized machine. The point considered in this current drive operation is located on the curve $n_e/n_{\rm Gr} = 0.9$ of the plane ($\langle n_e \rangle$, $P_{\rm add}$), and it corresponds to the maximum amplification factor Q with the constraint $\beta_{\rm N} \leq 2.5$. The helium fraction $f_{\rm He}$ is calculated self-consistently by imposing $\tau^*_{\rm He}/\tau_E = 6$.

Note that, as explained previously, the magnetic field on the plasma axis increases with the aspect ratio and, consequently, the minor plasma radius a is decreased for a given $Q = 5$ objective and constraints. The resulting major radius R

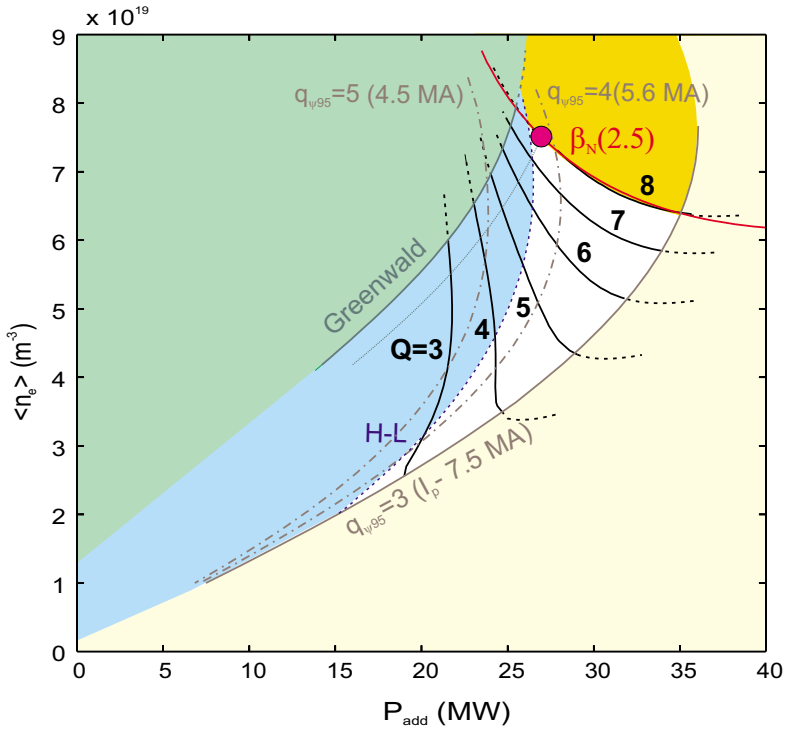

Figure 5.15: Current drive diagram of the $A = 3.5$ device considering an advanced tokamak regime ($H_{\mathrm{H}} = 1.4$ and $\alpha_n = 1.0$).

appears to be approximately constant in the range $5 - 5.2$ m. Therefore, the plasma volume V decreases significantly when A increases.

In view of the design and performance results, the following statements can be made:

- the operating space with good confinement, which is limited by MHD stability and H-L transition, is reduced when the aspect ratio increases;
- in inductive operation, the peak heat flux on the divertor target plates $\Phi_{\text{div-peak}}$ and the average neutron flux on the plasma surface Γ_n increase when the aspect ratio increases (the $A = 4$ machine overtakes the $\Phi_{\text{div-peak}} = 10$ MW/m^2 ITER-FEAT constraint);
- the amplification factor in non-inductive operation increases significantly from $Q \simeq 4.9$ to $Q \simeq 8.0$ when the aspect ratio goes from 3 to 4, mainly due to the increase of the bootstrap current fraction.

Finally, it must be borne in mind that the discharges corresponding to an aspect

Table 5.1: Characteristics of the inductive operating point corresponding to the optimized devices for aspect ratios 3, 3.5 and 4.

A	3.0	3.5	4.0
R (m)	5.24	5.00	5.02
a (m)	1.75	1.43	1.26
κ_{95}	1.71	1.63	1.54
κ_X	1.88	1.79	1.69
δ_{95} $(= \delta_X)$	0.35	0.35	0.35
V (m^3)	585	356	262
$B_{t\,\max}$ (T)	9.05	10.6	11.9
B_{t_0} (T)	4.31	5.43	6.56
I_p (MA)	11.3	8.96	7.53
$\langle n_e \rangle$ (10^{20} m^{-3})	1.06	1.25	1.36
$\langle T_e \rangle$ (keV)	6.44	7.50	8.83
P_{fus} (MW)	169	206	256
P_{add} (MW)	32.9	40.5	50.8
β_{N}	1.77	2.01	2.23
$P_{\text{sep}}/P_{\text{H-L}}$	1.22	1.20	1.20
Γ_n (MW/m^2)	0.26	0.41	0.60
$\Phi_{\text{div-peak}}$ (MW/m^2)	6.32	8.61	11.1

ratio of 4 are not well documented in the database used to establish the scaling laws for the energy confinement time or H-L transition.

On account of these elements, we are inclined to favour the machine with an intermediate aspect ratio: $A = 3.5$. Fig. 5.16 shows the radial build for the resulting M2 machine.

5.6 Estimation of synchrotron power losses

The evaluation of the error produced when neglecting the synchrotron losses term in the thermal equilibrium equation, is performed for the M2 ($A = 3.5$) operating point in the inductive mode of operation, i.e. taking the volume averaged density $\langle n_e \rangle = 1.25 \times 10^{20}$ m^{-3} (90% of the Greenwald limit) and electron temperature $\langle T_e \rangle = 7.5$ keV.

Synchrotron radiation losses P_{syn} are calculated using the new fit derived in Chapter 3, with reflection coefficients on the walls in the range $r = 0.7 - 1.0$.[3]

[3]The wall reflection coefficient $r = 1$ corresponds to the case where synchrotron losses in the thermal plasma equilibrium are neglected.

Table 5.2: Characteristics of the non-inductive optimal points at maximum Q and $n/n_{\rm Gr} = 0.9$, for the optimized devices at aspect ratios 3, 3.5 and 4 with an advanced regime.

A	3.0	3.5	4.0
$\beta_{\rm N}$	2.50	2.50	2.50
$n_e/n_{\rm Gr}$	0.90	0.90	0.90
$q_{\Psi 95}$	4.54	4.34	4.10
I_p (MA)	7.48	6.23	5.51
$f_{\rm He}$ (%)	2.99	3.46	4.15
$\langle n_e \rangle$ (10^{20} m^{-3})	0.53	0.66	0.75
$\langle T_e \rangle$ (keV)	8.67	8.95	9.57
Q	4.89	6.12	8.01
$P_{\rm fus}$ (MW)	210	206	216
$P_{\rm add}$ (MW)	43.0	33.7	27.0
$f_{\rm BS}$ (%)	64.0	70.5	75.2
$\Phi_{\rm div\text{-}peak}$ (MW/m^2)	9.22	8.95	7.83

Table 5.3 presents $P_{\rm syn}$, the ratio of $P_{\rm syn}$ to the total power losses, and the resulting amplification factor Q when solving the thermal plasma equilibrium for different values of the wall reflection coefficient. The rest of the assumptions are those used in the performance prediction in inductive mode of operation.

Note that in these conditions, when the density and temperature are fixed, the H-L transition margin and beta parameter are also fixed (see Eqs (2.9), (2.22), and (2.26)). Hence, for any wall coefficient reflection value we have $P_{\rm sep}/P_{\rm H\text{-}L} = 1.20$ and $\beta_{\rm N} \simeq 2.01$.

Table 5.3: Analysis of synchrotron losses for the M2 nominal point in inductive operation for $r = 0.7$, 0.8, 0.9 and 1.0.

r	0.7	0.8	0.9	1.0
$P_{\rm syn}$ (MW)	1.94	1.58	1.12	0.0
$P_{\rm syn}/P_{\rm losses}$ (%)	2.30	1.88	1.34	0.0
Q	4.81	4.85	4.90	5.0

We see that synchrotron losses represent less than 2.5% of the total losses (about 2.3% for $r = 0.7$ and about 1.3% for $r = 0.9$), and the amplification factor is reduced by less than 4% in the least favourable case ($r = 0.7$). In view of these results, we conclude that neglecting synchrotron losses in the optimisation algorithm has a negligible influence on the M2 design.

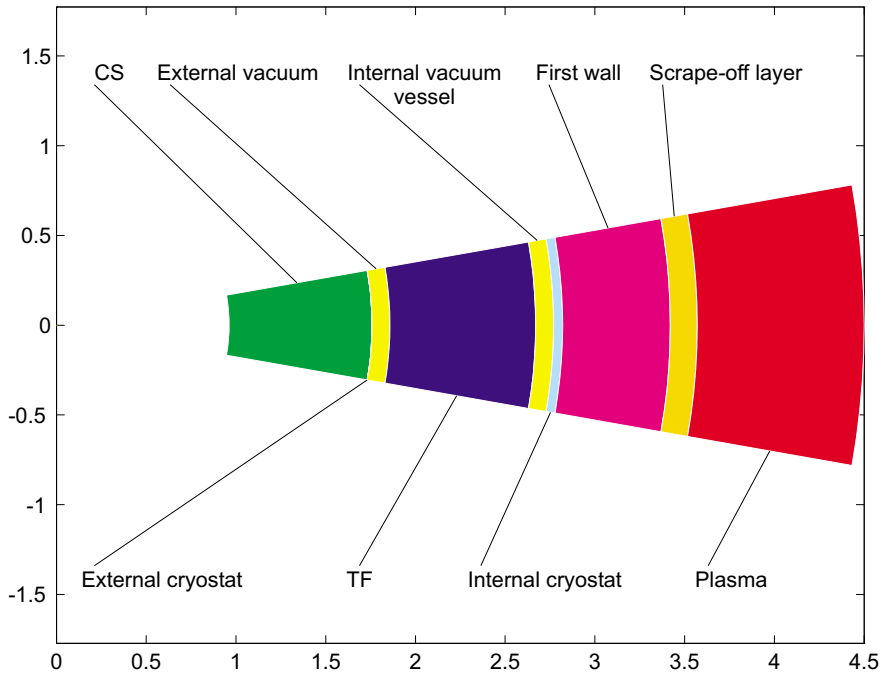

Figure 5.16: Radial build of the M2 machine ($A = 3.5$), from the plasma to the tokamak axis.

5.7 Additional considerations

An estimation of the electrical power required for the operation of the M2 machine ($A = 3.5$) has been made using the design basis presented above [Alb99a]. Where the toroidal magnet operation is concerned, the electrical power required can be considered negligible because of the superconducting properties. A power of 400 MW can be estimated for the poloidal circuit performing the function of magnetic field equilibrium control and stability and central solenoid. Adding 45 MW of plasma additional heating, the total electrical power required for the M2 operation is about 445 MW. Note that the electrical power required for the operation of a machine keeping the same plasma parameters of M2 but which is designed with copper magnets has been estimated to 1700 MW.

The investment cost of the M2 machine can be preliminary estimated. This evaluation is based on both the previous studies of present-day experimental devices (e.g. JET, Tore Supra), and the cost studies performed for important future tokamak projects (e.g. ITER, PCAST, TPX). Table 5.4 presents the partial cost by concept and the overall cost, which is about 1675 MEuros. More details about the determination of these costs are given in Ref. [Alb99b].

Finally, assuming 1000 shots of 500 seconds per year for 15 years, with 1/3 of the

Table 5.4: Cost estimate of the M2 components and total cost (in MEuros).

Concept	*Cost (MEuros)*
Toroidal magnets (18 coils)	361
Poloidal magnets	172
Building	229
Divertor and first wall	112
Blanket and vacuum chamber	107
Cryostat	17
TF (power supplies and protection)	15
PF (power supplies and protection)	37
High voltage (HV) distribution	45
Assembly and maintenance tools	127
Machine cooling	61
Magnet cooling	0
Control and diagnostics	75
Tritium, fuelling and pumping	137
Cryogenic system	46
Additional heatings (45 MW)	134
Total cost	1675

shots in D-T, and an average neutron flux Γ_n at the plasma surface of 0.41 MW/m^2 (see Table 5.1), we obtain a neutron fluence of about 0.033 MWy/m^2, much lower than that foreseen for ITER-FEAT [ODR99].

5.8 Summary

For three different aspect ratios ($A = 3, 3.5$ and 4), the smallest machine meeting the imposed physical and technological requirements is determined. In practice, the optimized point corresponds to $P_{\text{sep}}/P_{\text{H-L}} = 1.2$ (or close to this value for $A = 3$) and $\beta_{\text{N}} < 2.5$. The magnetic field on the plasma axis is limited by the mechanical constraints on the magnetic systems and by the available flux required to generate a plateau duration of 500 seconds. When the aspect ratio increases, the space available for the TF and CS increases, resulting in a higher magnetic field and a smaller plasma radius and volume.

The optimisation study for different aspect ratios is useful to understand trends in physical and technological feasibility. Hence, on the one hand, the operating space with good confinement is reduced when the aspect ratio increases and, in the inductive mode of operation, the peak heat flux on the divertor target plates as well as the average neutron flux on the plasma surface increase. On the other hand, the

amplification factor in non-inductive operation increases significantly from $Q \simeq 4.9$ to $Q \simeq 8.0$ when the aspect ratio goes from 3 to 4. On account of these elements, the machine with an intermediate aspect ratio ($A = 3.5$) has been retained as the M2 machine (which has a major radius of about 5 meters).

In inductive mode of operation, the design of M2 results in a machine with a moderate fusion power of about 200 MW, an additional heating power of about 40 MW, an average neutron flux at the plasma surface of about 0.4 kW/m^2, and a peak heat flux on the divertor target plates of about 8.6 MW/m^2. From a technological point of view, this machine, which is less ambitious than ITER, should not raise any particular problems. Its cost has been estimated at 1.7 billion Euros, which should be compatible with the European budget possibilities.